Piezoelectric Actuators as Synthetic Jets: Cavity Dimension Effects

Poorna Mane, Karla Mossi, Ali Rostami, Robert Bryant and Nicolas Castro

Journal of Intelligent Material Systems and Structures 2007; 18; 1175 originally published online May 30, 2007;
DOI: 10.1177/1045389X06075658

Piezoelectric Actuators as Synthetic Jets: Cavity Dimension Effects

POORNA MANE,[1] KARLA MOSSI,[1,*] ALI ROSTAMI,[1] ROBERT BRYANT[2] AND NICOLAS CASTRO[1]

[1] *Virginia Commonwealth University, 601 West Main Street, P.O. Box 843015 Richmond, Virginia 23284-3015, USA*

[2] *NASA Langley Research Center, 6 West Taylor St., B1293A Mail Stop 226, Hampton, VA 23681, USA*

ABSTRACT: Effects of dimensional cavity parameters, height, and orifice diameter, on synthetic jet peak velocities are investigated numerically and experimentally, utilizing two piezoelectric composite diaphragms, Bimorph and Thunder®. The system is modeled using a RNG κ–ε model with a mesh generated using a tri-pave unstructured scheme and the diaphragms are modeled as moving boundaries. The model compares within 15% for a Bimorph but underpredicts the results for Thunder® by more than 30%. For a Bimorph, both cavity parameters are relevant with the orifice diameter having a higher effect. For Thunder® however, only orifice diameter is found to be statistically significant.

Key Words: pre-stressed piezoelectric actuators, synthetic jet, Thunder®, Bimorph.

INTRODUCTION

METHODS that attempt to control the motion of fluids have been extensively explored in the past. These methods can be passive or active or both (Gad-el-Hak, 2000). Passive flow control is usually achieved through careful modifications to the existing system using rigid bodies such as wing flaps, spoilers, and vortex generators, among others. These techniques though effective are not capable of adjusting to the instantaneous flow conditions experienced during flight. Active flow control however, can adapt to the constantly changing conditions by using methods that introduce small amounts of energy locally to achieve non-local changes in the flow field with large performance gains (Kral et al., 1997; Smith and Glezer, 1998; Amitay et al., 1998; Gad-el-Hak, 2000). In spite of all the advantages, using active flow control devices usually adds complexity in design, and increases manufacturing and operation cost of the system preventing their use. For this reason, many researchers have focused on designing better active flow control devices that are easy to manufacture, are small in size, and require little power to operate. One device that fulfills all these qualities is called synthetic jets. Synthetic jets consist of a cavity with an oscillating diaphragm. When the diaphragm oscillates, air is pushed out an orifice forming a jet (Smith, 1999). The interaction of the jets with an external flow leads to the formation of closed re-circulating flow regimes near the surface, which can act as a 'virtual surface' and consequently to an apparent modification of the flow boundary (Amitay et al., 1997; Utturkar et al., 2003).

The oscillating diaphragm is usually driven using electrical or mechanical power. In the past, researchers have used compressed air or regulated blowers as a means of supplying steady or oscillating flow (Seifert et al., 1993, 1996; Smith and Swift, 2003). This adds to the complexity and weight of the system. Piezoelectric disks as oscillating diaphragms offer an alternative to these techniques and several investigators use these devices as diaphragms for synthetic jets in attempts to make the systems lighter, increase efficiency, and save resources (Rathnasingham and Breuer, 1997a,b; Smith and Glezer, 1998; Crook et al., 1999).

Crook et al. constructed a device, a piezoelectric disc bonded to a brass shim, based on preliminary analysis by Rathnasingham and Breuer that modeled a thin circular plate as a piston. Results showed the model provided a good prediction of the mean value of the velocity in the developed jet though the model did not predict the peak centerline jet velocity. Similar devices have been considered by Smith et al. in a number of studies referenced throughout this article. Although Smith et al. have been successful in generating high velocities capable of altering the flow fields, the devices

*Author to whom correspondence should be addressed.
E-mail: kmmossi@vcu.edu
Figures 1–3 appear in color online: http://jim.sagepub.com

1045-389X/07/11 1175–16 $10.00/0 DOI: 10.1177/1045389X06075658

operate at high frequencies consequently requiring high power to operate. More sophisticated systems that are now available include sensors and feedback controls as demonstrated by Tian et al. (2006). Their work uses an adaptive feedback disturbance rejection algorithm applied in conjunction with a piezoelectric synthetic jet actuator and surface mounted unsteady pressure transducers to control the separated flow. Though their work shows that a single actuator consumes only 27 mW of power, the controls and pressure transducers require more power and add weight to the system. Other recent studies have concentrated on high-aspect-ratio planar synthetic jets and their usefulness for active flow control applications (Abdou and Ziada, 2006). Formation, evolution, and interaction between jets are aspects that have been studied experimentally by Smith and Glezer (2005). In short, there is a vast number of studies on synthetic jets and their effectiveness; however, the focus of this study is on the driving section of the synthetic jet, the active diaphragm.

In the current study, piezoelectric composites are used as active diaphragms in the jet cavity. In addition to active piezoelectric layers they have reinforcing layers of metal or other stronger materials which give them added durability. These actuators have the ability to produce micro scale displacements. They have fast response times and they are also lightweight. These advantages make them suitable for flow control purposes as demonstrated by Mossi and Bryant (2004a) and Schaeffler et al. (2002). Several synthetic jet designs have been developed by Schaeffler et al. in an attempt to integrate them into an airfoil for wind tunnel testing. In these models, careful consideration has been given to the size constraints imposed on the devices. Preliminary wind tunnel tests proved them to have a lot of potential but it was determined that further research into this concept was required.

Piezoelectric diaphragms are usually driven using alternating fields such that jets are formed as a result of volumetric displacement within a fluid-filled cavity. As the actuator oscillates it alternately draws in and blows out the ambient fluid through either a high aspect ratio slot or an axisymmetric circular orifice on the cavity. During the suction part of the cycle, the diaphragm moves away from the orifice drawing in ambient fluid to fill the increasing volume within the cavity. During the ejection cycle, the diaphragm moves toward the orifice pushing fluid out of the cavity. Some of the vortices formed at the edge of the slit or orifice will travel sufficiently far and escape re-entrainment during the suction cycle resulting in a synthetic jet with a net momentum and zero net mass flux (Smith, 1999).

The promising potential of piezoelectric synthetic jets for flow control has motivated researchers at various universities and government institutions to continue to invest time and effort to shed insight into their functionality. Synthetic jets have potential applications ranging from thrust vectoring jet engines (Smith and Glezer, 1998), mixing enhancement, (Chen et al., 1999; Davis and Glezer, 1999) to active control of separation and turbulence in boundary layers (Amitay et al., 1997, 1998; Crook et al., 1999). Development of practical applications using this technology requires extensive research into their performance under various conditions since its performance depends on the geometry of the jet cavity, the oscillating diaphragm used, and electrical driving conditions amongst other things. Little understanding exists as to how performance characteristics scale with these parameters. In the current study, piezoelectric synthetic jets in quiescent air are investigated for specific cases both numerically and experimentally.

Two composite piezoelectric actuators, Bimorph and Thunder®, are utilized. The composite actuators are different in construction and thus in the way they displace. The Bimorph is made up to two PZT discs with adhesive in between the layers making the device displacement simulate a piston like displacement (Mossi and Bryant, 2004b).

Alternately the Thunder® device consists of three high-temperature bonded layers of different materials that result in a saddle shape (Mossi et al., 1998). Owing to its shape and other actuator properties, the Thunder® device has a non-uniform displacement which is very complex to model (Hyer and Schultz, 2004). Thunder® has been the subject of intense investigation (Capozzoli et al., 1999; Granger et al., 2000; Ballato et al., 2001; Lee et al., 2002; Aimmanee and Hyer, 2004; Lee et al., 2004; Usher and Sim, 2005; Yoon et al., 2005; Goo et al., 2005; Taleghani and Campbell, 1999; Wieman et al., 2001) due to their unique performance characteristics compared to a Unimorph® and a Bimorph device, as well as traditional direct extensional actuators. Benjeddou et al. (1997) attempted to investigate the factors that contribute to the improved performance of these devices investigating mass loading effects, engineering mechanics effects, and hysteresis effects. Smith et al. (2003) attributed these actuators' improved performance to enhanced domain switching.

Thus the displacement profiles and amplitudes are quite different and empirical regression equations are developed to be incorporated into the numerical models. These models are developed using the geometry and mesh generator GAMBIT version 2.1, and numerical fluid modeling software FLUENT version 6.1. The selected numerical results are validated with experimental measurements.

The objective of this research is to explore the effects of cavity geometry, cavity height, and orifice diameter, on the performance of piezoelectric composite actuators as synthetic jets. By using a two-level experimental

design, velocity profiles formed at the orifice exit are used as the establishing criteria. Previous work has demonstrated that cavity height and orifice dimensions are important parameters affecting the performance of the jet (Crook et al., 1999; Baysal et al., 2004; Mossi et al., 2005; Mossi and Bryant, 2004c). Baysal et al. utilized a design of experiments methodology to show that the width of the actuator cavity and the frequency of its oscillations are the most effective design variables. All their conclusions were based on numerically obtained data.

In this study, the focus is on understanding the dependence of the jet on cavity dimensional parameters, frequencies using a sinusoidal driving signal, and the actuator type. In this manner through the utilization of high and low values of the different tested parameters, both the numerically and experimentally obtained results are evaluated. This type of approach, based on design of experiments theory, can be utilized to statistically evaluate the relevance of the parameters that may be significant to the performance of the synthetic jet such that a complete theoretical development can be pursued.

EXPERIMENTAL SETUP

This section describes the composition of the actuator used, Bimorph and Thunder®, as well as the setup used in the experiments. The Bimorph, model T216-A4NO-573X is manufactured by Piezoelectric Systems Inc. and consists of two bonded 63.5 mm diameter piezoelectric discs with nickel electrodes, a total thickness of 0.41 mm, and capacitance of 130 nF as shown in Figure 1.

The Thunder® is a pre-stressed curved Unimorph® manufactured by Face International and composed of three layers, a top perforated copper layer 0.0254 mm thick, a middle piezoelectric layer of thickness 0.254 mm, and a bottom 0.254 mm thick layer of stainless steel. The layers of 63.5 mm diameter are laminated with a high temperature polyimide adhesive (Bryant, 1996) through a layering high-temperature bonding process (Mossi et al., 1998). The resulting actuator is saddle shaped with a capacitance of 100 nF as shown in Figure 2. The piezoelectric ceramic used in both these diaphragms is a soft PZT type 5A.

The cavity used as a synthetic jet is shown in Figure 3. This cavity setup allows variations in cavity height and orifice dimensions. The two cavities have overall dimensions of $89.0 \times 89.0 \times 19.1\ \text{mm}^3$ and $89.0 \times 89.0 \times 15.1\ \text{mm}^3$, which correspond to cavity heights of 9.5 and 5.5 mm, respectively. This cavity height, C_H, is measured from the diaphragm to the orifice exit. The cavity housing is composed of two identical rectangular Plexiglas™ pieces with a circular aperture and a cover plate with an orifice. The two plastic pieces have 3.18 mm deep circular grooves along the circumference of the aperture. The diaphragm is placed in this groove between the two pieces with neoprene rubber around the perimeter of the diaphragm on either side. Seven 3.18 mm screws hold the two plastic housings and the cover plate together and clamp the actuator in place. Two cover plates with circular orifices having

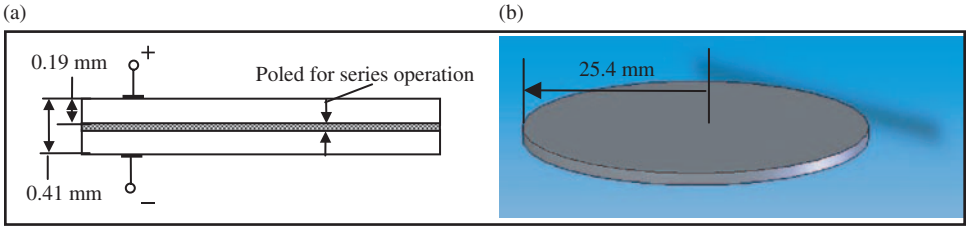

Figure 1. *Bimorph specifications: (a) layer characteristics and (b) final shape.*

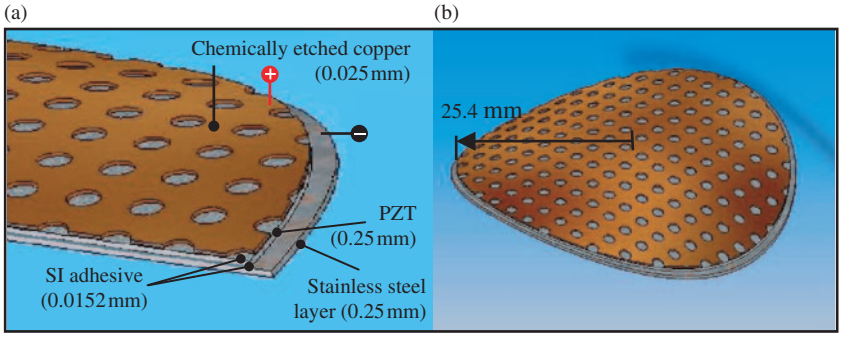

Figure 2. *Thunder® configuration: (a) layer characteristics and (b) final shape.*

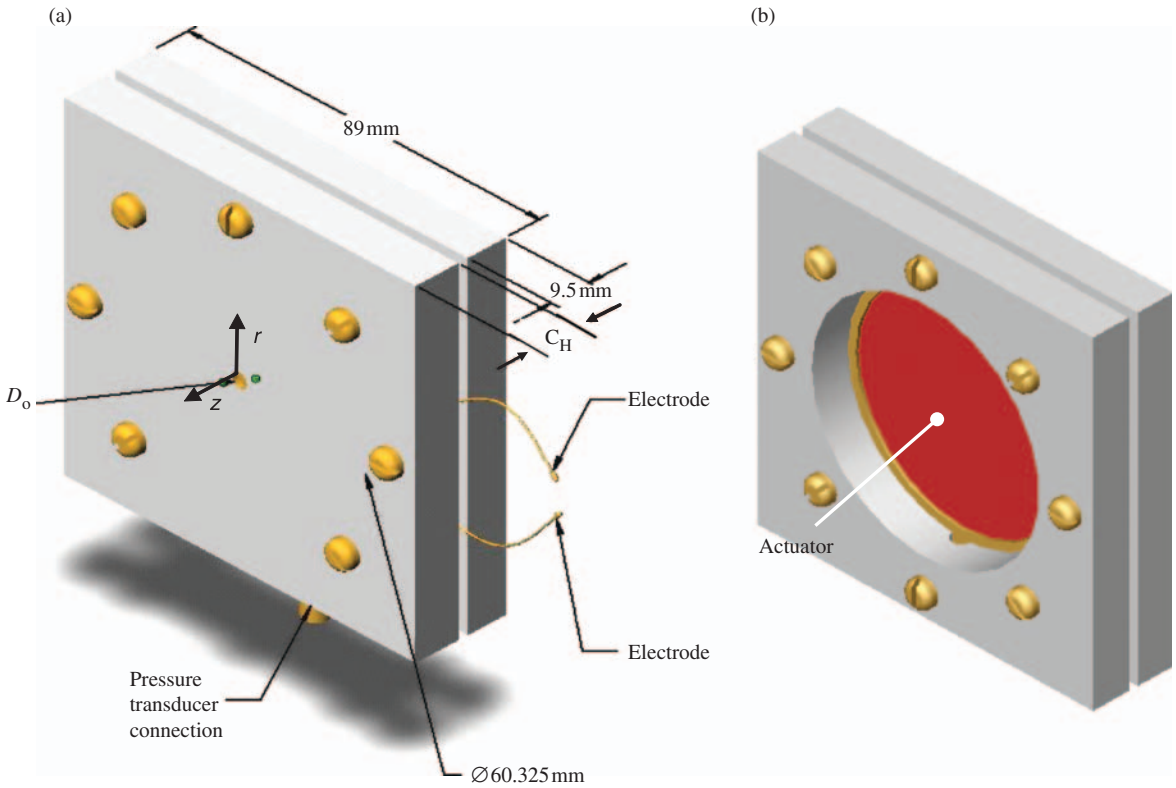

Figure 3. *Synthetic jet cavity: (a) final assembly and (b) clamped actuator.*

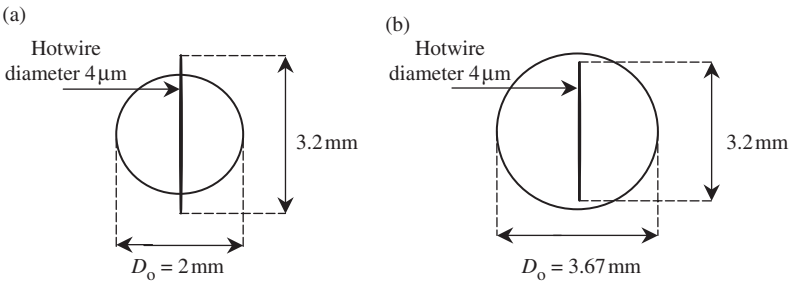

Figure 4. *Hot-wire dimensions with respect to the synthetic jet orifice: (a) small orifice and (b) large orifice.*

approximate diameters, D_o, of 2.0 mm (small) and 3.67 mm (large) are used.

The assembled actuator-cavity is mounted onto an adjustable height gage, with the actuators surface perpendicular to the hot-wire anemometer used to measure velocity of the jet. The IFA100 hot-wire anemometer has a diameter of 4 µm and a length of 3.2 mm. It can be traversed through the diameter of the synthetic jet orifice as shown in Figure 4.

A sinusoidal driving signal is applied at high voltages and varying frequencies for each device (150Vpp for Bimorph and 400Vpp for Thunder®). This signal is applied using a signal generator, an HP model HP33120, connected to an amplifier, TREK model PZD700. The velocity and voltage signals are monitored and recorded using an oscilloscope, LeCroy model 350L and a National Instruments data acquisition system as shown in Figure 5. The magnitude of the applied signal and the frequency are kept below their allowable maximum driving fields and their respective resonant frequencies in order to prevent electrical and mechanical failure of the diaphragms. Velocities are measured in quiescent air in the z-direction at specific locations along the diameter of the circular orifice.

NUMERICAL MODELING

The modeling of synthetic jets cavities is complex since it requires knowledge of the displacement field produced by the diaphragms. Hence the modeling is a blend of numerical and experimental work as described in the following sections. The commercial CFD software, Fluent 6.1, and the corresponding geometry and

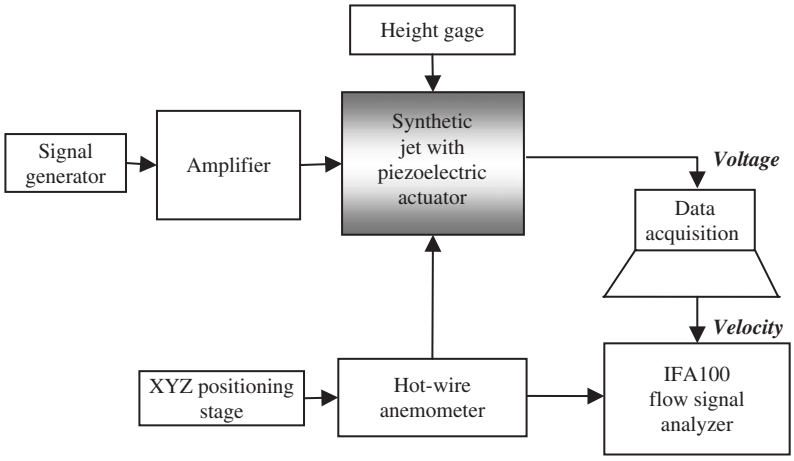

Figure 5. *Experimental layout.*

mesh generating software, Gambit 2.1, were used for numerical modeling.

The problem is axisymmetric, two-dimensional, unsteady state, non-swirling, isothermal flow with no mass and momentum sources. The compressibility effects are accounted for.

Governing Equations

The equation of mass conservation, or continuity equation, for 2D axisymmetric geometries, with unsteady flow with no swirling effects may be written as:

$$\frac{\partial \rho}{\partial t} + \frac{\partial}{\partial z}(\rho u) + \frac{\partial}{\partial r}(\rho v) + \frac{\rho v}{r} = 0. \tag{1}$$

Equation (1) is valid for incompressible as well as compressible flows with no mass source term. z is the axial coordinate and r is the radial coordinate. u and v are the velocities in the corresponding directions.

The axial and radial momentum equations for 2D axisymmetric flow with no body force may be written as shown in Equations (2a) and (2b).

$$\begin{aligned}\frac{\partial}{\partial t}(\rho u) + \frac{1}{r}\frac{\partial}{\partial z}(r\rho u^2) + \frac{1}{r}\frac{\partial}{\partial r}(r\rho uv) \\ = -\frac{\partial p}{\partial z} + \frac{1}{r}\frac{\partial}{\partial z}\left[r\mu\left(2\frac{\partial u}{\partial z} - \frac{2}{3}(\Delta \cdot \boldsymbol{V})\right)\right] \\ + \frac{1}{r}\frac{\partial}{\partial r}\left[r\mu\left(\frac{\partial u}{\partial r} + \frac{\partial v}{\partial z}\right)\right]\end{aligned} \tag{2a}$$

$$\begin{aligned}\frac{\partial}{\partial t}(\rho v) + \frac{1}{r}\frac{\partial}{\partial z}(r\rho uv) + \frac{1}{r}\frac{\partial}{\partial r}(r\rho v^2) \\ = -\frac{\partial p}{\partial r} + \frac{1}{r}\frac{\partial}{\partial r}\left[r\mu\left(2\frac{\partial v}{\partial r} - \frac{2}{3}(\Delta \cdot \boldsymbol{V})\right)\right] \\ + \frac{1}{r}\frac{\partial}{\partial z}\left[r\mu\left(\frac{\partial u}{\partial r} + \frac{\partial v}{\partial z}\right)\right] - 2\mu\frac{v}{r^2} + \frac{2}{3}\frac{\mu}{r}(\Delta \cdot \boldsymbol{V})\end{aligned} \tag{2b}$$

where,

$$\Delta \cdot \boldsymbol{V} = \frac{\partial u}{\partial z} + \frac{\partial v}{\partial r} + \frac{v}{r}.$$

Boundary Conditions

The boundary conditions for the boundaries specified in Figure 6 are as follows:

Surface 1: u is given by the moving boundary as described in the next section, $v = 0$

Surfaces 2, 3, 4, and 5: $u = v = 0$

Surface 6 (at large radial distance): constant ambient pressure (inlet to domain)

Surface 7 (at large axial distance): constant ambient pressure (outlet from domain).

Geometry and Mesh

The synthetic jet cavity is assumed to consist of three regions that include the cavity, the orifice, and the ambient air into which the jet exits. Boundary conditions are then specified for each of the edges that comprise the cavity and the ambient fluid into which the jet is expelled. The diaphragm and cavity surfaces are considered as impermeable walls as shown in Figure 6; the ambient air is specified with two pressure inlets and one pressure outlet. The diaphragm is defined separately from the rest of the walls so that a user-defined function can be used to describe its movement. These conditions are specified by using GAMBIT 2.1.

The problem can be adequately represented by a 2D axisymmetric system. Size functions to control and specify the size of the mesh spacing intervals between nodes are attached to the orifice edge, orifice exit vertex, and the diaphragm upper vertex. This ensures fine meshing in the regions where large gradients are present. After applying the size functions, the computational domain is meshed using the tri-pave unstructured

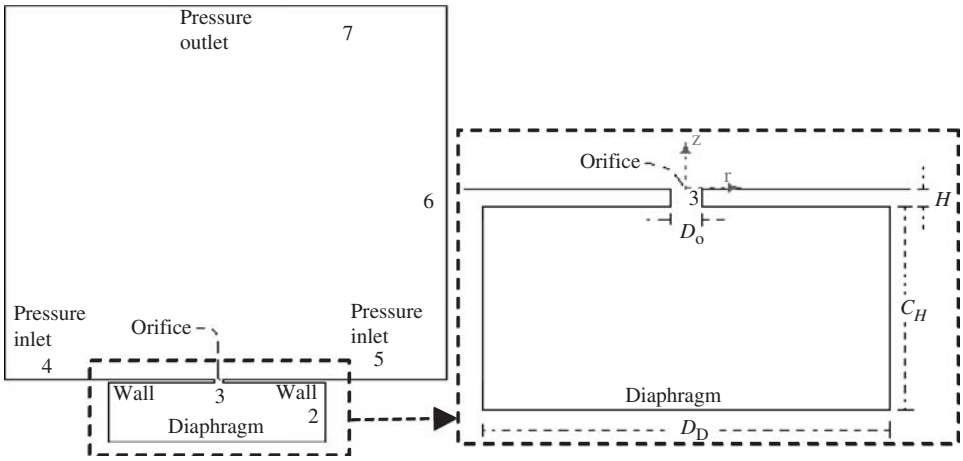

Figure 6. *Synthetic jet geometry and boundary conditions.*

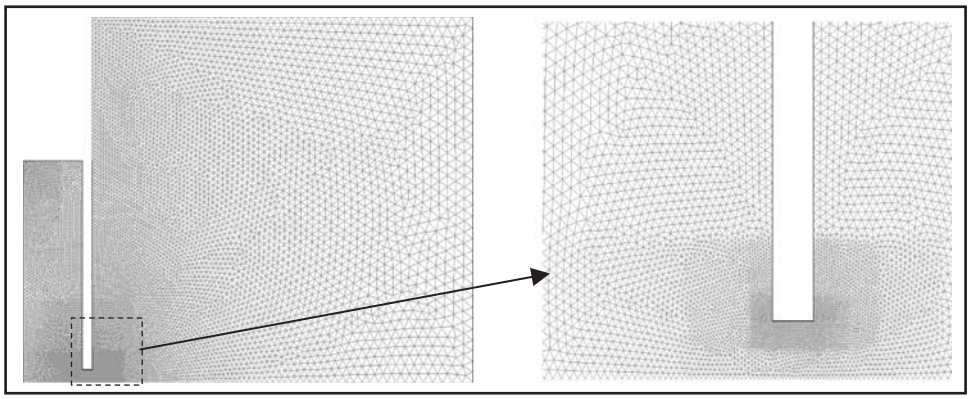

Figure 7. *Synthetic jet mesh.*

scheme that results in the following mesh arrangement shown in Figure 7.

The tri-pave unstructured scheme is chosen to allow for relative displacement among the nodes on the diaphragm that is necessary and not possible with the structured quadrilateral scheme.

FLUENT Parameters

The mesh developed in Gambit is exported into FLUENT, which uses a control-volume-based technique to convert the governing Navier–Stokes equations (Equations (1) and (2)) at each node cell into algebraic equations that can be solved through iteration. Values are stored at the cell center and the face values needed for the convective term are interpolated from center values. Diffusion terms are central-differenced and are always second-order accurate.

The segregated, unsteady, axisymmetric solver is chosen with first-order implicit time scheme that is unconditionally stable with respect to time step size. The segregated solver mainly solves the resulting algebraic equations sequentially as opposed to the coupled solver that solves the algebraic equations simultaneously.

The turbulence model used in this study is based on the results presented by Zhong et al. (2004). In their work, the RNG 'renormalization group'$\kappa-\varepsilon$ model produced the best results.

Pressure-implicit with splitting of operators (PISO) based on a higher degree of approximation between the iterative corrections for pressure and velocity is chosen. This algorithm also significantly reduces convergence difficulties associated with a highly distorted skewed mesh with approximately the same number of iterations that would be required for a more orthogonal mesh.

Second-order upwind spatial discretization is used for the momentum, turbulent kinetic energy, turbulent dissipation rate, and energy. Owing to nonlinearities it is necessary to control the calculated value change to assure proper convergence through the use of under-relaxation parameters. The default under-relaxation parameters were kept at 0.3, 1.0, and 0.7 for pressure, density, and momentum, respectively.

The solution is then initialized at the diaphragm with initial value of zero for the gage pressure, axial velocity, and radial velocity. For the turbulent κ–ε RNG model turbulent specifications for the pressure inlet and outlet boundary are set using the intensity and

length scale with values of 2% intensity and a length scale of 0.35 mm and the initial guess for turbulent kinetic energy and turbulent dissipation rate are set to $0.05\,m^2/s^2$ and $0.05\,m^2/s^3$, respectively.

The default of 20 maximum iterations per time step is kept. A time step is chosen based on the actuation frequency to allow for 200 time steps per cycle as shown in Equation (3).

$$\Delta t = \frac{1}{f^*200} \tag{3}$$

where f is the frequency of vibration of the diaphragm in Hertz.

DIAPHRAGM BOUNDARY CONDITIONS

Successful computational fluid dynamics (CFD) synthetic jet flow simulations that incorporate the oscillating piezoelectric diaphragms displacement performance depend heavily on accurate approximations of the displacement profiles, including the instantaneous deflections and shape modes. One of the earliest studies by Rathnasingham and Breuer (1997a,b) modeled the oscillating diaphragm as a simple rigid piston to approximate volumetric changes in the cavity without considering the actual temporal and spatial displacement profile of the oscillating diaphragm. This approach does not guarantee an accurate description of instantaneous volumetric changes. In this study, a moving boundary is utilized instead of a velocity boundary and therefore approximations for the moving field are evaluated.

Logarithmic Approximation

In this section, the instantaneous oscillatory displacement of the diaphragm due to a sinusoidal input as a function of time and radial position, $\delta(r,t)$, is approximated by a logarithmic profile. For the logarithmic profile, the instantaneous displacement is described by Equation (4) (Timoshenko, 1959). This equation was used by Tang and Zhong (2005) while using a magnetic shaker as the driving force. The profile is used as a moving boundary condition to simulate the oscillations of the diaphragm as shown in Equation (4).

$$\delta(r,t) = \frac{\delta_C}{2}\left[1 - \frac{4r^2}{D_D^2} + \frac{8r^2}{D_D^2}\ln\left(\frac{2r}{D_D}\right)\right]\sin(2\pi ft) \tag{4}$$

where δ_C is the diaphragm center, peak-to-peak displacement, r is the radial distance from the center of the diaphragm, D_D is the diaphragm diameter, and f is the actuation frequency. Differentiating Equation (4) the instantaneous logarithmic diaphragm velocity is derived as shown in Equation (5).

$$u(r,t) = \pi\delta_C f\left[1 - \frac{4r^2}{D_D^2} + \frac{8r^2}{D_D^2}\ln\left(\frac{2r}{D_D}\right)\right]\cos(2\pi ft). \tag{5}$$

The above equations, coupled with the mesh, geometry, and numerical simulations are performed using Fluent. The experimentally measured and numerically used peak-to-peak center diaphragm displacement, δ_C, for the Bimorph actuator is 0.396 mm (Mossi and Bryant, 2004b). The results are validated by experimentally measuring a velocity waveform at two randomly selected frequencies in one time period. A typical result for a Bimorph actuator is shown in Figure 8(a). In the case of 32 Hz frequency the numerical and experimental profiles are in good agreement. For 50 Hz, the results are slightly different in magnitude but follow a similar trend. To quantify the variations, percentage differences between numerical and experimental maximum velocity values are compared; for 32 Hz, the numerical and experimental data are within 3%; and for 50 Hz,

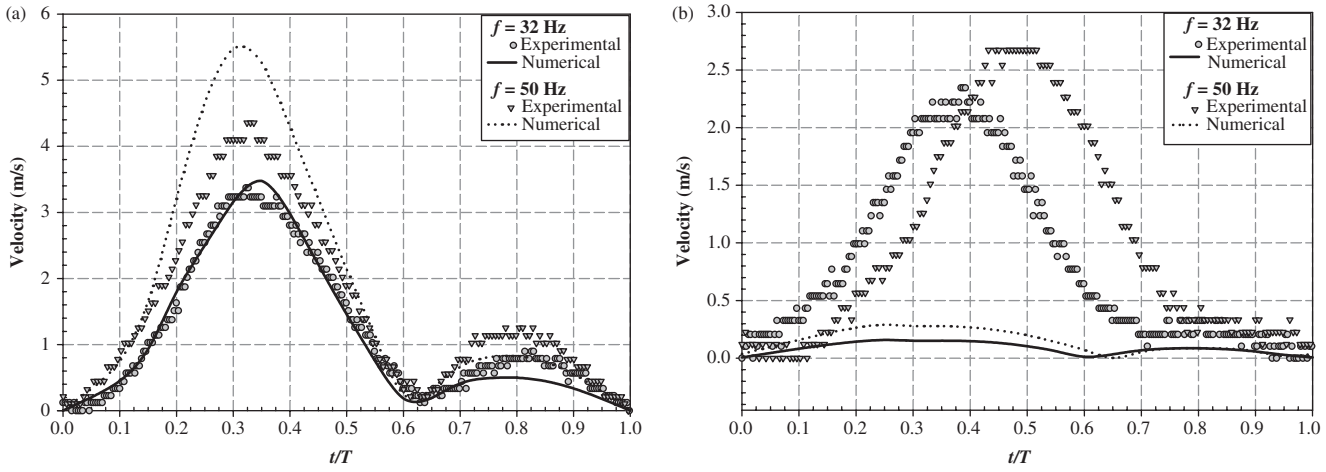

Figure 8. *Logarithmic profile: (a) Bimorph and (b) Thunder®.*

the results are within 21%. Based on these results, the logarithmic profile is considered as a good approximation of the device performance.

For the Thunder® device however, the results using the logarithmic profile are not in agreement at any tested frequency as shown in Figure 8(b). The differences between the experimental and numerical results at both 32 and 50 Hz are >93% and hence not in agreement. These results may be due to the complex shape and performance of this pre-stressed actuator. The next section describes the changes made to the displacement profile using experimental results.

Modified Profile for a Thunder® Device

Owing to the shape of the Thunder® device a logarithmic profile does not serve as a good approximation for the displacement profile. Mossi and Bryant (2004b) mapped the surface of the device clamped around its perimeter, at rest and under a constant DC voltage. By performing a regression along the centerline of the device, a parabolic approximation of the form shown in Equation (6) predicted the displacement to have a parabolic shape.

$$\delta(x,y) = y_o + Ax + By + Cx^2 + Dy^2 \tag{6}$$

where y_o, A, B, C, D are constants, x and y are the coordinates of the device's surface, and $f(x,y)$ is the displacement obtained. The axisymmetric counterpart may be written as:

$$\delta(r) = a + b \cdot \left[\frac{r}{D_D/2}\right] + c \cdot \left[\frac{r}{D_D/2}\right]^2. \tag{7}$$

Performing non-linear regression analysis of the variable coefficients of Equation (7) leads to further optimization of the equation. The regression in Table 1 shows the p-value (probability of the value being significant with a 95% confidence) is not significant for the parameter b, reducing Equation (7) to Equation (8).

$$\delta(r) = a - c\left(\frac{r}{(D_D/2)}\right)^2. \tag{8}$$

The maximum displacement, δ_C, occurs at the center of the device, while the zero displacement is maintained at the perimeter. That is:

$$\delta(0) = \delta_C/2$$
$$\delta(D_D/2) = 0.$$

Therefore,

$$\delta(r) = \delta_C\left(1 - \left(\frac{r}{(D_D/2)}\right)^2\right). \tag{9}$$

A comparison between these equations and the experimentally obtained results is plotted in Figure 9. It is important to note that these equations are valid with no load on the devices and are only an approximation since the devices have a three-dimensional shape that may require a more complex equation to describe its performance. Once the description of the magnitude of the displacement is performed, the time component of the displacement is added.

Time component is usually a sinusoidal waveform. In this case however, the device at time = 0 has a particular value, a dome-height. When a positive voltage is applied to this device, the dome height diminishes or the device flattens. Therefore, a cosine function instead of a sine function can more accurately describe the devices displacement performance with time. By re-arranging Equations (8) and (9), adding a time component, Equation (10) is obtained.

$$\delta(r,t) = \left[(f\pi\delta_C)\cdot\cos(2\pi ft) - (f\pi\delta_C)\cdot\cos(2\pi ft)\left(\frac{r}{(D_D/2)}\right)^2\right]. \tag{10}$$

Table 1. Analysis of variance for a Thunder® displacement profile.

Nonlinear regression equation: quadratic					
R	***R²***	**Adjusted *R²***		**Standard error of estimate**	
0.9985	0.997	0.9965		0.0579	
	Coefficients	Standard error	*t*	*P*	VIF
a	1.2938	0.0210	61.6242	<0.0001	2.6319
b	−0.0483	0.0212	−2.2720	0.0364	1.0591
c	−0.9250	0.0427	−21.6625	<0.0001	2.7205
Analysis of variance					
	DF	SS	MS		
Regression	3	19.0475	6.3492		
Residual	17	0.0569	0.0033		
Total	20	19.1045	0.9552		

Differentiating Equation (10), a condition for velocity is obtained as shown in Equation (11).

$$u(r,t) = \left[-f\pi\delta_C \cdot \sin(2\pi ft) + (f\pi\delta_C) \cdot \sin(2\pi ft) \left(\frac{r}{(D_D/2)} \right)^2 \right] \tag{11}$$

where δ_C is the experimentally and numerically used peak-to-peak center displacement for the Thunder® actuator, which is 0.07 mm. The profile described by Equation (10) is compared with experimental data at 32 and 50 Hz, like in the case of a logarithmic profile. The results shown in Figure 10(a) and (b) at 32 and 50 Hz, respectively show a better similarity in trend and magnitude than the logarithmic profile. The error at 32 Hz in predicting maximum velocity is 26 and 28% at 50 Hz. Though the error is still high, this profile better approximates the results and will be used to test the cavity parameter effects on velocity.

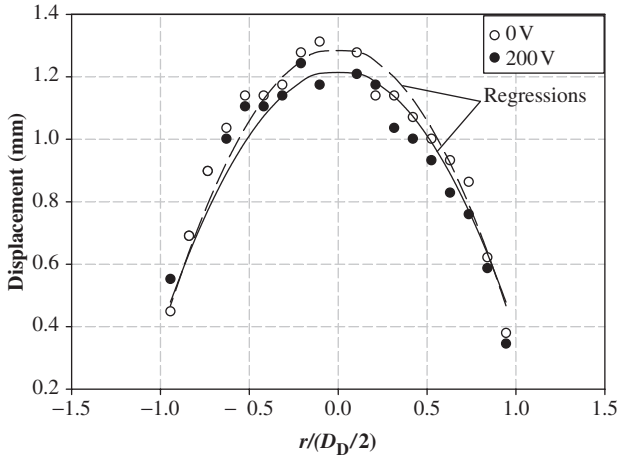

Figure 9. *Displacement profile for a Thunder® device.*

CAVITY PARAMETER EFFECTS

Different cavity configurations, shown in Table 2, are tested to study the effects of cavity height and orifice diameter on the jet velocity. The numerically obtained velocity profiles are compared with experimental results. The comparisons are based on the magnitudes of the jet velocities. The two piezoelectric diaphragms are modeled according to the profiles described in the previous sections.

Bimorph

Numerical simulations of the synthetic jet cavity serve as a tool to study flow characteristics that are hard to experimentally measure. In the case of velocity vector plots, the direction of the flow at a particular instant in time is possible. For instance, in the case of a Bimorph, Figure 11(a) and (b) shows the maximum and minimum positions of the diaphragm for the cavity IV case which has the largest dimensions. At the maximum position, Figure 11(a), the direction of the flow is mixed since some of the flow is going inside the cavity and is what is sometimes denominated as the injection cycle. This type of reversed flow is not possible to measure with a single hot-wire anemometer that measures unidirectional flow. However, as demonstrated by Yao et al. (2004) a hot-wire anemometer at locations not close to exit slot, match closely the results from particle image velocimetry (PIV) and laser Doppler velocimetry (LDV). At the minimum position, Figure 11(b), the expulsion position, vortices are formed and a jet is formed through the center.

To illustrate the differences in the formed jet by changing the cavity physical dimensions, a velocity vector plot for a cavity of different dimensions, cavity I

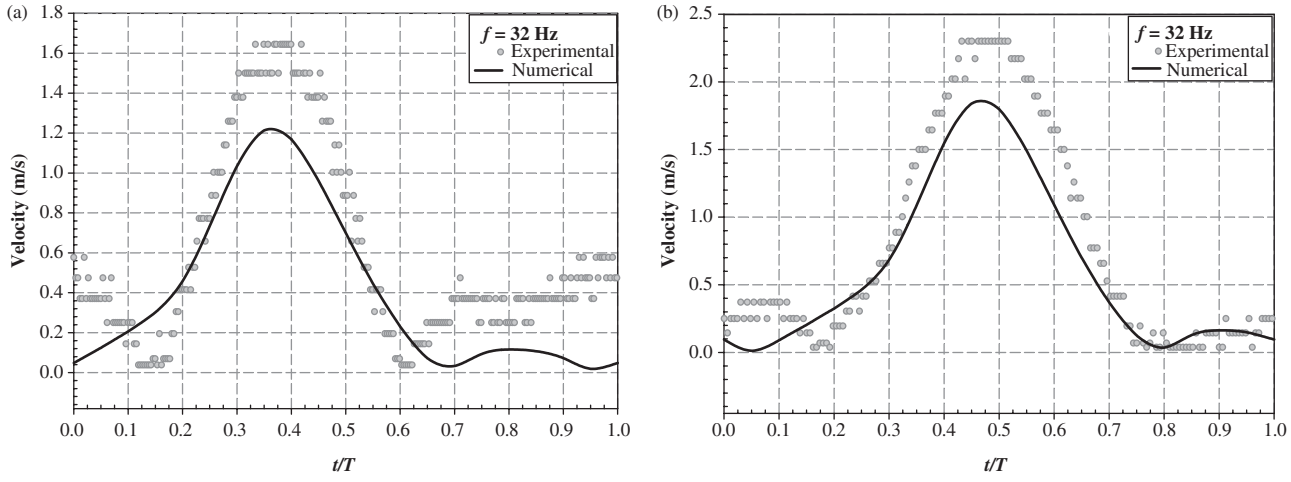

Figure 10. *Parabolic profile for a Thunder® device: (a) 32 Hz and (b) 50 Hz.*

with the smallest D_o and C_H, the same maximum and minimum diaphragm positions are shown in Figure 12(a) and (b), respectively. At the maximum position, the injection cycle, all the flow is unidirectional unlike Cavity IV, where the flow is bidirectional. At the minimum position, the expulsion cycle, the flow is forming a defined jet.

Bimorph positions are defined as: (1) maximum volume at $t=0$ occurs when the diaphragm is at its lowest point (furthest from orifice; $t=0$) and the cavity has maximum fluid volume; (2) maximum expulsion ($t=0.25T$) corresponds to when the diaphragm is at level position and moving with maximum velocity toward the orifice; (3) minimum volume occurs halfway through the cycle ($t=0.5T$) when the diaphragm is at the highest position (closest to orifice) and the volume of

Table 2. Cavity parameters.

		C_H (mm)	
		5.50	**9.55**
D_o (mm)	2.00	Cavity I	Cavity II
	3.67	Cavity III	Cavity IV

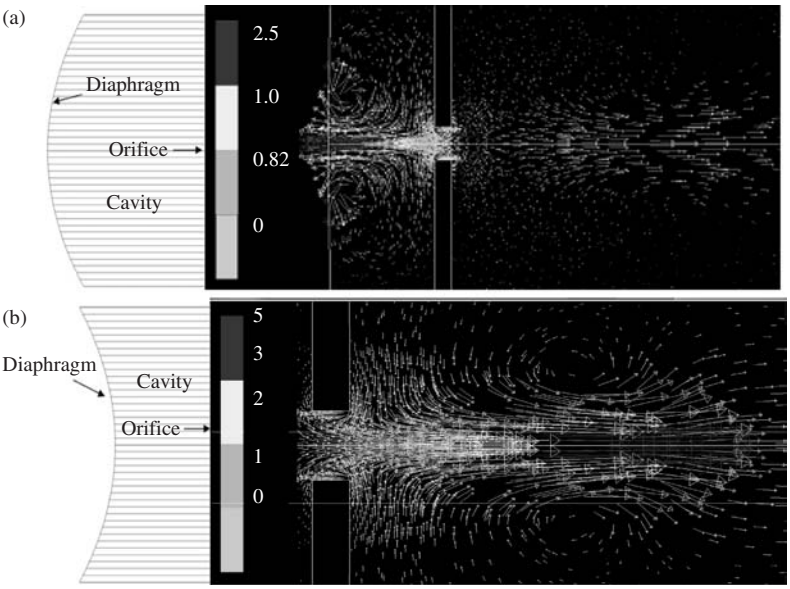

Figure 11. *Velocity vector plots for a Bimorph in cavity at: (a) maximum cavity volume and (b) minimum cavity volume.*

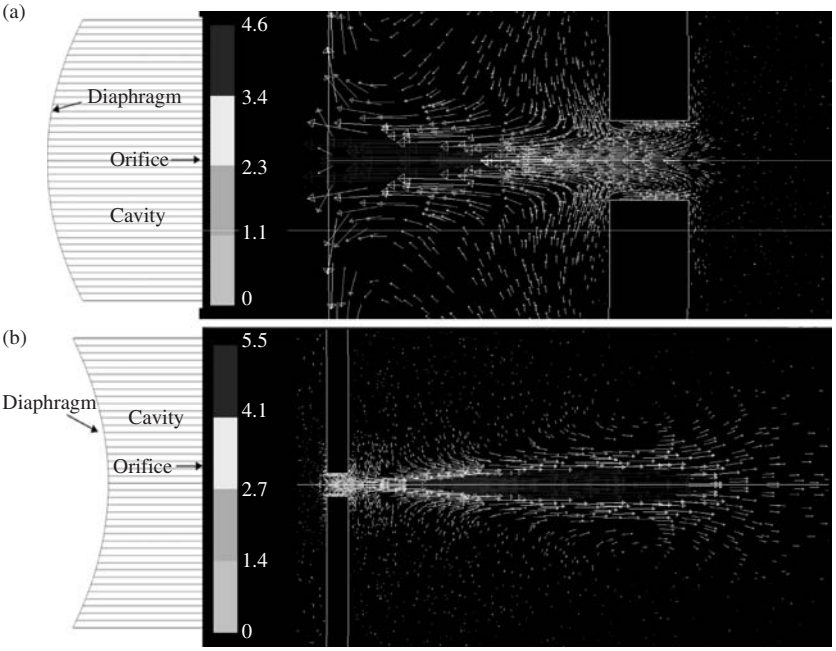

Figure 12. *Velocity vector plots for a Bimorph in cavity I at: (a) maximum diaphragm position and (b) minimum diaphragm position.*

fluid in the cavity is at a minimum; and (4) maximum ingestion ($t = 0.75T$) corresponds to when the diaphragm is at level position and moving with maximum velocity away from the orifice. The numerical profiles for these times are illustrated in Figure 13 where for clarity purposes, the experimental data are removed.

Similar to the numerical profiles, experimentally the velocity profile along the radius of the orifice is mapped for each cavity. Profiles at $t = 0.25T$ or maximum expulsion cycle, are compared to the measured velocity profiles for cavities IV and I as shown in Figure 14(a) and (b), respectively. Cavity IV velocity profile at the axial distance of 2 mm and the diaphragm frequency of 50 Hz is shown in Figure 14(a). The model overpredicts the experimental results for the Bimorph actuator in cavity IV by 25%.

The numerical and experimental results for cavity I were also compared as shown in Figure 14(b). In the case of cavity I the outer extremes of the numerical and experimental profiles do not match. These differences in velocity magnitudes ($r/D > 0.6$) could be due to the hotwire inability of detecting flow direction. The higher maximum experimentally measured velocities observed in the outer portion of the jet most likely occurs during the ingestion cycle when the fluid flow is from the outer edges. If the negative numerical values attained during the ingestion cycle were entered as the absolute values in the velocity profile of maximum ingestion it would give a wider jet to resemble that of the experimental results. The numerical results overpredict the maximum measured experimental velocity at 50 Hz by only 10%.

In order to test the effects of changes in cavity height and orifice diameter the profiles obtained from the four cavities were compared. Since cavities IV and III have the same orifice diameter but different cavity heights their profile comparison will show the effects of changes in cavity height or cavity volume on the velocity magnitudes.

Profiles for cavities IV and III shown in Figure 15, at $t = 0.25T$ is maximum expulsion for the numerical model. It is observed that the maximum numerical velocity obtained between the largest cavity height (cavity IV) and the smallest cavity height (cavity III) is

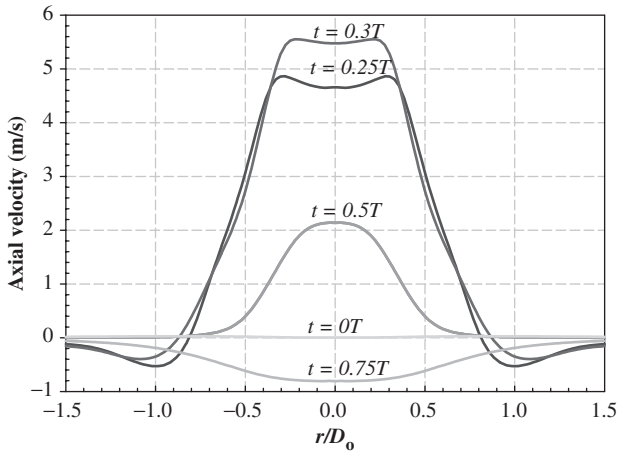

Figure 13. *Numerical axial velocity vs radial position at z = 2 mm for a Bimorph at different times in cavity IV: (t = 0T) maximum volume, (t = 0.25T) maximum expulsion, (t = 0.3T) maximum velocity, (t = 0.5T) maximum volume, and (t = 0.75T) maximum ingestion.*

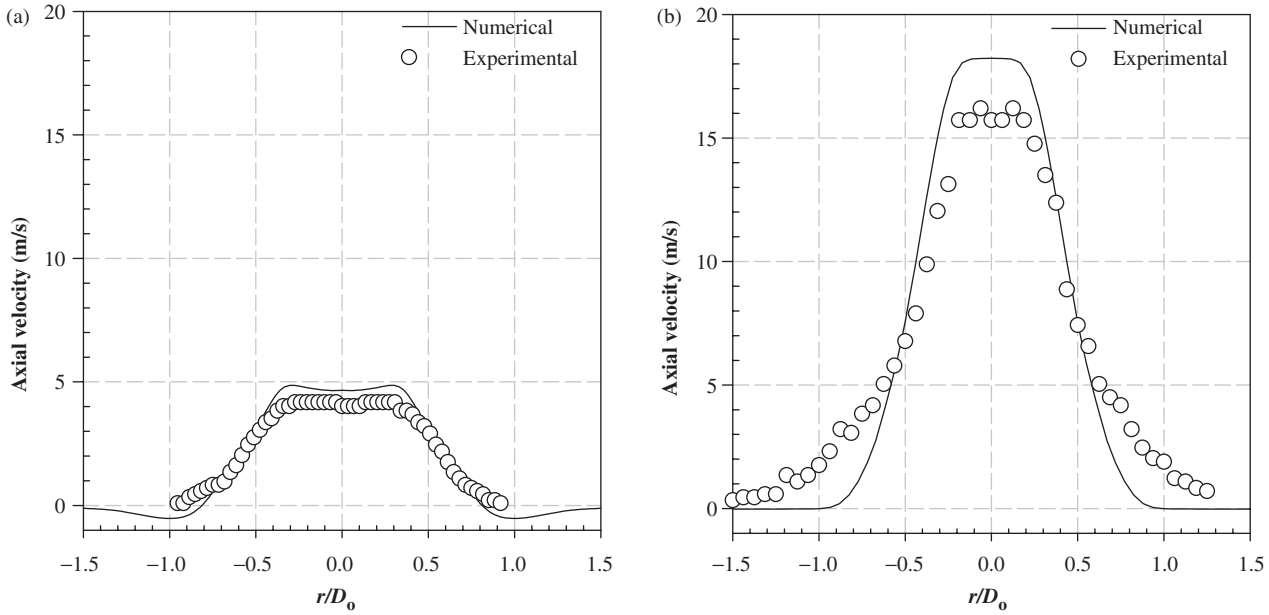

Figure 14. *Numerical and experimental axial velocity profile for a Bimorph at z = 2 mm and 50 Hz at maximum expulsion for: (a) cavity IV, largest C_H, and D_0 and (b) cavity I, smallest C_H, and D_0.*

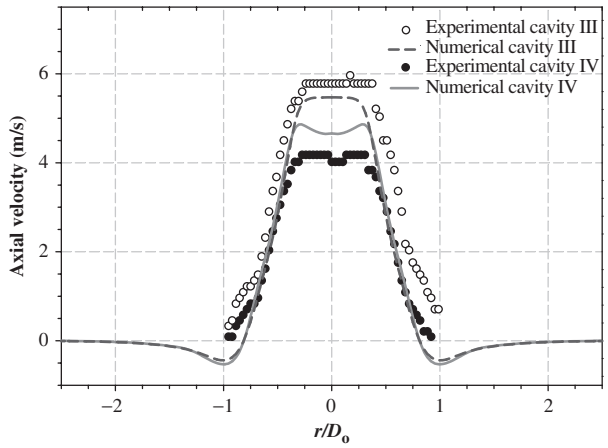

Figure 15. *Cavity height effects on a Bimorph device at z = 2 mm and 50 Hz.*

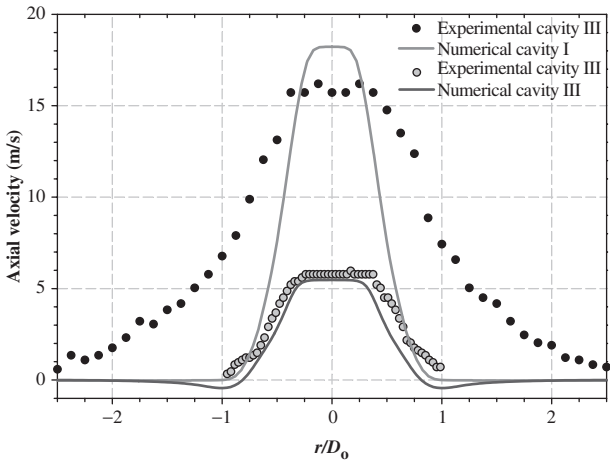

Figure 16. *Orifice size effects for a Bimorph at z = 2 mm and 50 Hz.*

≈11% for the cases shown (larger D_o), and 1% for the case of cavities I and II (smallest D_o).

Next the effects of orifice size on jet velocity are studied. Figure 16 shows the profiles for cavities I and III that have the same cavity height (smaller C_H) but different orifice diameters. The numerical and experimental profiles are comparable in shape but not in magnitude with differences of $< 15\%$ when comparing average maximum velocities. It is observed that the smallest D_o, cavity I, produces higher velocities than cavity III, highest D_o. This could be because cavity I has a smaller orifice as compared to cavity III and in order to maintain a constant mass flow rate, the velocity through the smaller orifice has to be higher than the larger orifice. Similar trends are observed in the comparison between cavities IV and II (largest C_H).

Based on the cavity height and orifice diameter comparisons for the Bimorph, it can be said that for the current synthetic jet configuration orifice diameter has a larger effect on the velocities produced by the jet.

The effects of frequency on the jet velocity were also studied. The graph of the maximum center velocity versus frequency at an axial distance of 2 mm for cavity I is shown in Figure 17. It is seen that as the frequency increases the velocity also tends to increase until it reaches a constant value close to its resonant frequency. The model gives a good approximation diverging only toward the higher frequencies. This may be due to the driving frequency approaching the resonant frequency of the actuator. The model does not account for the resonance effects on the actuators.

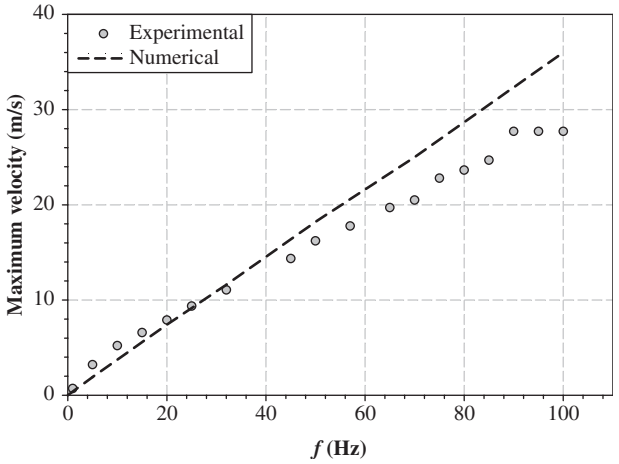

Figure 17. *Frequency effects on a Bimorph cavity I.*

Thunder®

The following section is for the Thunder® actuator in the four cavity configurations. In this case, the parabolic profile is used such that the displacement is entirely away from the orifice. This modification is used to account for the pre-stressed shape of a Thunder® actuator.

In the modified parabolic displacement profile the diaphragm begins at the level position or minimum volume at $t = 0T$. It then moves away from the orifice and reaches the maximum ingestion, $t = 0.25T$, which corresponds to the position where the diaphragm is moving with maximum velocity away from the orifice, at $t = 0.5T$; the diaphragm reaches the lowest point maximum volume, with a center distance of 0.07 mm below the level point. The maximum expulsion occurs at $t = 0.75T$ when the diaphragm is moving with maximum velocity toward the orifice before returning to the level position or minimum volume at $t = 1T$. Figure 18 shows a summary of all the numerical profiles obtained at the prescribed times described.

The radial velocity profile plots for cavity IV experimental and numerical are shown in Figure 19(a).

It is seen that the model gives a fair approximation of the experimental values for the Thunder® actuator in the cavity IV configuration. As opposed to cavity IV, the model does not approximate the cavity I experimental results as shown in Figure 19(b).

Axial velocity numerical simulations for the Thunder® actuator in any cavity are underestimated by more than 34% indicating that this particular actuator type in numerical simulations require more than a 2D approach for an approximation of its displacement performance. This fact coupled with the pressures developed inside the cavity, as shown in Figure 20, makes numerical predictions incomplete. The pressure inside the cavity might load the device in such a manner that the displacement of the actuator behavior is altered significantly.

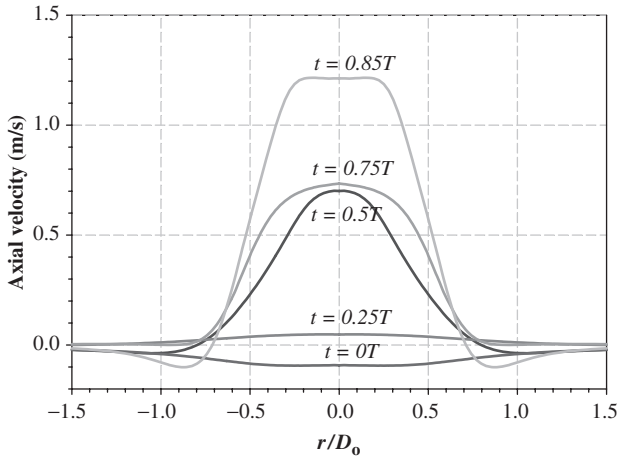

Figure 18. *Numerical velocity profiles vs radial position for a Thunder® in cavity IV at z = 2 mm and 32 Hz at different positions: (t = 0T) minimum volume, (t = 0.25T) maximum ingestion, (t = 0.5T) maximum volume, (t = 0.75T) maximum expulsion, and (t = 0.85T) maximum velocity.*

Experimental Results

Experimentally obtained profiles for the four tested configurations are shown in Figure 21. By observing the results, profiles obtained with cavities IV and III, and cavities I and II, only one effect is evident for the Thunder® device and that is the cavity height. These results are similar to the Bimorph results. To provide a picture of the effects of varying the two factors chosen, cavity height, C_H, and orifice diameter, D_o, a simple two-factor full factorial analysis can be performed on the results for both the Thunder® and the Bimorph. The experimental results for both actuators can then be analyzed by using basic factorial design analysis (Montgomery, 2005). A two-factor full factorial is of the form of 2^2 numbers of experiments. A simpler analysis can be performed by choosing one response variable at one specific frequency and location, that is, peak velocity. These values are shown in Table 3. In this table, a minus value denominates the lowest value of either cavity height, C_H, or diameter of the orifice D_o. A plus sign denominates the highest value respectively.

Experiment numbers I through IV correspond to the four different cavities studied. To determine the main effects on peak velocity, an average response to each of the considered factors can be calculated as well as to evaluate the presence of an interaction between the factors. The value of the effect of each factor, ΔF_{C_H} and ΔF_{D_o}, is calculated by using Equation (12).

$$\Delta F = \frac{1}{2}\sum_{i=1}^{n=4} \text{response}_i \cdot \text{Factors}_i. \qquad (12)$$

For instance, in the case of the experimental data for a Bimorph, the effect of cavity height is larger than

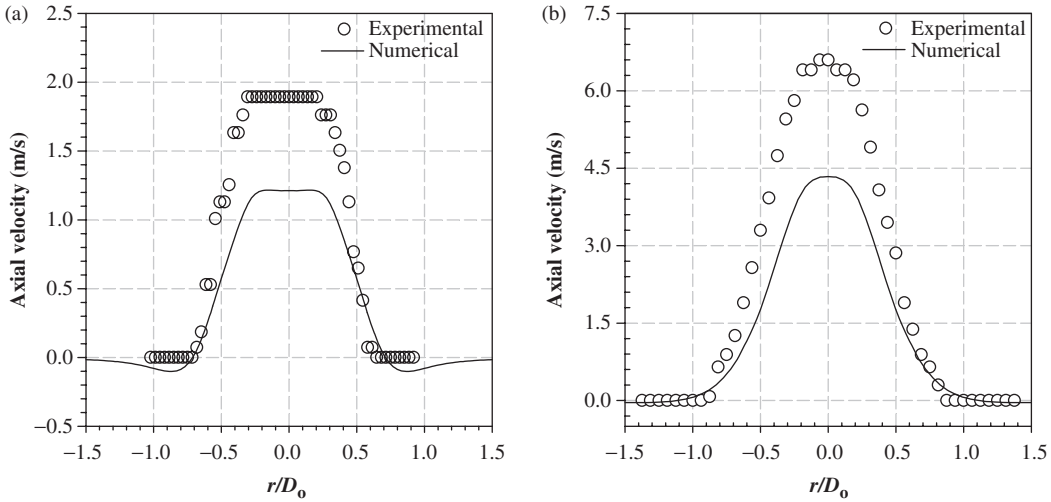

Figure 19. *Axial velocity vs radial position at z = 2 mm and 32 Hz for: (a) cavity IV and (b) cavity I.*

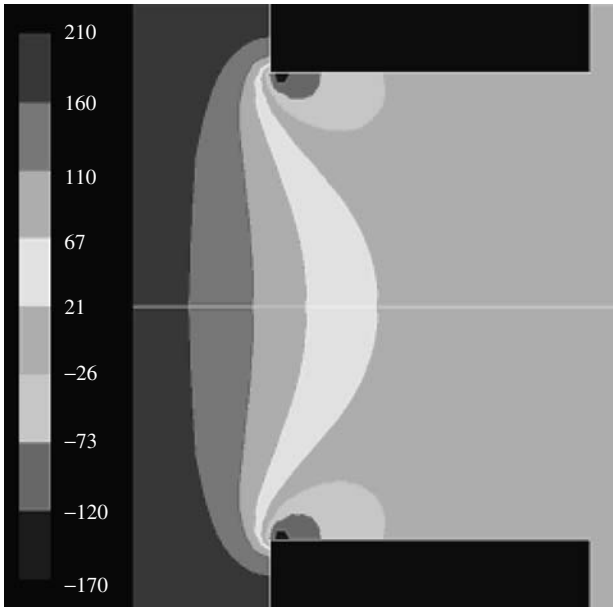

Figure 20. *Typical pressure distributions inside a cavity.*

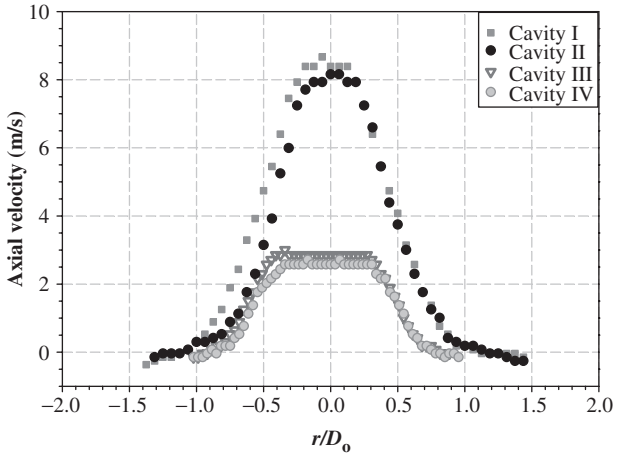

Figure 21. *Experimental cavity comparison for Thunder® at 50 Hz.*

orifice diameter, but not insignificant as shown in Equations 13(a) and (b).

$$\Delta C_{\mathrm{H}}(\text{Thunder}) = \frac{1}{2}\cdot[-8.669 + 8.157 - 3.001 + 2.713] = -0.4 \quad (13a)$$

and

$$\Delta D_{\mathrm{o}}(\text{Thunder}) = \frac{1}{2}\cdot[-8.669 - 8.157 + 3.001 + 2.713] = -5.56. \quad (13b)$$

These results indicate that the effect of cavity height is minimal compared to the orifice diameter effect on maximum velocity. Similarly, for a Bimorph, the results are for cavity height −3.5, and for orifice diameter −8.5, indicating an interaction between effects. That is, both parameters are important ones to be considered when optimizing this device for velocity. These coefficients that evaluate the relevance of the parameters, and numerical results indicate that optimization of a synthetic jet cavity is strongly coupled to the type of piezoelectric composite utilized and the knowledge of its displacement field.

Table 3. Factorial design 2^2 at $z = 2$ mm and 32 Hz with peak velocity in m/s as response.

	Factors		Experimental	
Cavity	C_H	D_o	Thunder®	Bimorph
I	−	−	8.669	16.195
II	+	−	8.157	10.759
III	−	+	3.001	5.779
IV	+	+	2.713	4.177

CONCLUSIONS

This study included axisymmetric numerical simulations and experimental measurements of synthetic jet cavities using a piezoelectric diaphragm. The piezoelectric diaphragms modeled were a Bimorph and a Thunder®. A Bimorph consists of two layers of PZT and a Thunder® consists of a composite of copper, PZT, and stainless steel. To model deflection of these actuators as moving boundary conditions, two oscillating deflection profiles were used, parabolic for the Thunder® actuator and logarithmic for the Bimorph. Both actuators were tested in synthetic jet cavities that consisted of a combination of cavity heights and orifice diameters. For these cavities, the turbulent RNG κ–ε numerical model was used, geometry was setup using Gambit 2.1, and the numerical fluid modeling software FLUENT 6.1 is used for the flow analysis. Numerical results for the four cavity configurations were compared to experimental results.

The numerical formulation of the problem includes most of the relevant physical phenomena. Full Navier–Stokes equations with allowances for compressibility and turbulence have been solved. The errors were minimized by using small time steps and variable mesh sizes (smaller near steep changes and larger at more uniform regions). The major source of difference between the simulation results and the experiment data may be attributed to the uncertainty in the modeling of the moving wall boundary (diaphragm), which is used as boundary condition to the equations. The best approximation available in the literature was used, but it is admitted that each device has its unique performance, and it is hard to find a universally accepted wall motion formulation that can adequately represent all devices.

The simulated results for the Bimorph diaphragm were in good agreement with the experimental data with

differences up to ≈15%. A comparison between the cavity dimensional parameters showed that though the cavity height has a lower effect than orifice diameter on the jet velocity both effects need to be considered when optimizing a synthetic jet cavity with this device.

Since the logarithmic profile did not match the experimental profiles for the Thunder® device, a parabolic profile derived from experimental displacement maps is utilized. Though the results improved, numerical simulations still underpredicted experimental results by at least 30%. This could be due to the initial pre-stressed shape of the actuator and the pressure developed inside the cavity that loads the device, changing the shape of the assumed profile. Furthermore, contrary to the Bimorph where both parameters were significant, for the Thunder® device the orifice diameter is more relevant than cavity height on maximum synthetic jet velocity.

It was concluded that optimizing a synthetic jet cavity required knowledge of the displacement performance of the piezoelectric composite diaphragm. Hence, such optimization has to be performed according to the type of diaphragm utilized.

ACKNOWLEDGMENTS

The authors would like to acknowledge the support of NASA Langley Research Center, contract number NNL04AA04G, and Justin Maddox for his technical assistance.

REFERENCES

Abdou, S. and Ziada, S. 2006. "Spanwise Characteristics of High-Aspect-Ratio Synthetic Jets," *AIAA Journal*, 44(7): 1516–1523.

Aimmanee, S. and Hyer, M.W. 2004. "Analysis of the Manufactured Shape of Rectangular THUNDER-type Actuators," *Smart Materials & Structures*, 13(6):1389–1406.

Amitay, M., Honohan, A., Trautman, M. and Glezer, A. 1997. "Modification of the Aerodynamic Characteristics of Bluff Bodies using Fluidic Actuators," *AIAA Paper*, 1997–2004.

Amitay, M., Smith, B. and Glezer, A. 1998. "Aerodynamic Flow Control using Synthetic Jet Technology," *AIAA Paper*, 98–0208.

Ballato, J., Schwartz, R. and Ballato, A. 2001. "Network Formalism for Modeling Functionally Gradient Piezoelectric Plates and Stacks and Simulations of RAINBOW Ceramic Actuators," *IEEE Transactions on Ultrasonics, Ferroelectrics, and Frequency Control*, 48(2):462–476.

Baysal, O., Koklu, M. and Erbas, N. 2004. "Design of Micro Synthetic Jet Actuator for Flow Control," *Transport Phenomena in Micro and Nano Devices*. Kona, Hawaii, Oct. 17–21.

Benjeddou, A., Trindade, M.A. and Ohayon, R. 1997. "A Unified Beam Finite Element Model for Extension and Shear Piezoelectric Actuation Mechanisms," *Journal of Intelligent Material Systems and Structures*, 8:1012–1025.

Bryant, R. 1996. "LaRC-SI: A Soluble Aromatic Polyimide," *High Performance Polymers*, 8(4):607–615.

Capozzoli, M., Gopalakrishnan, J., Hogan, K., Massa, J., Tokarchik, T., Wilmarth, S., Banks, H.T., Mossi, K.M. and Smith, R.C. 1999. "Modeling Aspects Concerning THUNDER® Actuators," In: *Proc. of the Int. Soc. for Opt. Eng.*, 3667:719–727.

Chen, Y., Liang, S., Aung, K., Glezer, A. and Jogoda, J. 1999. "Enhanced Mixing in a Simulated Combustor Using Synthetic Jet Actuators," *AIAA Paper*, 1999–0449.

Crook, A., Sadri, A.M. and Wood, N.J. 1999. "The Development and Implementation of Synthetic Jets for the Control of Separated Flow," *AIAA Paper*, 1999–3176.

Davis, S.A. and Glezer, A. 1999. "Mixing Control of Fuel Jets using Synthetic Jet Technology," *AIAA Paper*, 1999–0447.

Gad-el-Hak, M. 2000. *Flow Control: Passive, Active, and Reactive Flow Management*, Chapter 1, Cambridge University Press, Cambridge, United Kingdom.

Goo, N.S., Haris, A., Park, H.C. and Yoon, K.J. 2005. "Validation of a Laminated Beam Model of Lipca Piezoelectric Actuators," *Journal of Intelligent Material Systems and Structures*, 16:189–195.

Granger, R., Washington, G. and Kwak, S.K. 2000. "Modeling and Control of a Singly Curved Active Aperture Antenna using Curved Piezoceramic Actuators," *J. of Intelligent Material Systems and Structures*, 11(3):225–233.

Hyer, M. and Schultz, M. 2004. "A Morphing Concept Based on Unsymmetric Composite Laminates and Piezoceramic MFC Actuators," *AIAA Paper*, 2004–1806.

Kral, L.D., Donovan, J.F., Cain, A.B. and Cary, A.W. 1997. "Numerical Simulation of Synthetic Set Actuators," *28th AIAA Fluid Dynamics Conference*, 97–1824, Reno, NV.

Lee, S., Cho, B.C., Park, H.C., Goo, N.S. and Yoon, K.J. 2004. "Piezoelectric Actuator-sensor Analysis using a Three-dimensional Assumed Strain Solid Element," *Journal of Intelligent Material Systems and Structures*, 15(5):329–338.

Lee, S., Cho, B.C., Park, H.C., Yoon, K.J. and Goo, N.S. 2002. "Analysis of Multi-layered Actuators using an Assumed Strain Solid Element," *Materials Chemistry and Physics*, 75(1–3): 174–177.

Montgomery, D. 2005. *Design and Analysis of Experiments*, 6th edn, John Wiley & Sons, Hobeken, NJ.

Mossi, K. and Bryant, R. 2004a. "Characterization of Piezoelectric Actuators for Flow Control over a Wing," *Actuator*, 2004:181–185.

Mossi, K. and Bryant, R. 2004b. "Pre-stressed Circular Actuators," *Ceramic Transactions*, 150:445–454.

Mossi, K. and Bryant, R. 2004c. "Piezoelectric Actuators for Synthetic Jet Applications," *Mat. Res. Soc. Symp. Proc.*, Vol. 785, 407–412.

Mossi, K., Mane, P. and Bryant, R. 2005. "Velocity Profiles for Synthetic Jets Using Piezoelectric Circular Actuators," *AIAA Paper*, 2005–2341.

Mossi, K., Selby, G. and Bryant, R. 1998. "Thin-layer Composite Unimorph Ferroelectric Driver and Sensor Properties," *Materials Letters*, 35:39–49.

Rathnasingham, R. and Breuer, K.S. 1997a. "Coupled Fluid-structural Characteristics of Actuators for Flow Control," *Phys. Fluids*, 9(7):1867–1869.

Rathnasingham, R. and Breuer, K.S. 1997b. System Identification and Active Control of a Turbulent Boundary Layer, AIAA 1997–1793.

Schaeffler, N.W., Hepner, T.E., Jones, G.S. and Kegerise, M.A. 2002. "Overview of Active Flow Control Actuator Development at NASA Langley Research Center," *AIAA Paper*, 2002–3159.

Seifert, A., Bachar, T., Koss, D., Shepshelovich, M. and Wygnanski, I. 1993. "Oscillatory Blowing: A Tool to delay Boundary-Layer Separation," *AIAA Journal*, 31(11):2052–2060.

Seifert, A., Darabi, A. and Wygnanski, I.1996. "Delay of Airfoil Stall by Periodic Excitation," *Journal of Aircraft*, 33(4):691–699.

Smith, B. and Swift, G. 2003. "A Comparison Between Synthetic Jets and Continuous Jets," *Experiments in Fluids*, 34:467–472.

Smith, B.L. 1999. Synthetic Jets and their Interaction with Adjacent Jets, PhD Thesis, Georgia Institute of Technology, p. 143.

Smith, B.L. and Glezer, A. 1998. "The Formation and Evolution of Synthetic Jets," *Physics of Fluids*, 10:2281–2297.

Smith, B.L. and Glezer, A. 2005. "Vectoring of Adjacent Synthetic Jets," *AIAA Journal*, 43(10):2117–2124.

Smith, R.C., Seelecke, S., Ounaies, Z. and Smith, J.A. 2003. "Free Energy Model for Hysteresis in Ferroelectric Materials," *Journal of Intelligent Material Systems and Structures*, 14:719–739.

Taleghani, B.K. and Campbell, J.F. 1999. "Non-linear Finite Element modeling of THUNDER Piezoelectric Actuators NASA Smart Structures and Materials," *Smart Structures and Integrated Systems*, 3668:555–566.

Tang, H. and Zhong, S. 2005. "Development of a Prediction Model for Synthetic Jets in Quiescent Conditions," AIAA 2005–104.

Tian, Y., Song, Q. and Cattafesta, L. 2006. "Adaptive Feedback Control of Flow Separation," *AIAA Paper*, 2006–3016.

Timoshenko, S. 1959. *Theory of Plates and Shells*, 2nd edn, McGraw-Hill, New York.

Usher, T. and Sim, A. 2005. "Nonlinear Dynamics of Piezoelectric High Displacement Actuators in Cantilever Mode," *Journal of Applied Physics*, 98(6):064102–064107.

Utturkar, Y., Holman, R., Mittal, R., Carroll B., Sheplak, M. and Cattafesta, L. 2003. "A Jet Formation Criteria for Synthetic Jet Actuators," *AIAA Paper*, 2003–0636.

Wieman, R., Smith, R.C., Kackley, T., Ounaies, Z. and Bernd, J. 2001. "Displacement Models for THUNDER Actuators having General Loads and Boundary Conditions," In: *Proc. of the Int. Soc. for Opt. Eng.*, 4326:253–263.

Yao, C., Chen, F., Harris, J., Newhart, D., 2004. "Synthetic Jet Flow Field Database for CFD Validation," AIAA-2004-2218.

Yoon, H.S., Washington, G. and Danak, A. 2005. "Modeling, Optimization, and Design of Efficient Initially Curved Piezoceramic Unimorphs for Energy Harvesting Applications," *Journal of Intelligent Material Systems and Structures*, 16(10): 877–888.

Zhong, S., Garcillan, L., Pokusevski, Z. and Wood, N. 2004. "A PIV Study of Synthetic Jets with Different Orifice Shape and Orientation," *AIAA Paper*, 2004–2213.